ISSN 0036-0236, Russian Journal of Inorganic Chemistry, 2015, Vol. 60, No. 12, pp. 1560–1567. © Pleiades Publishing, Ltd., 2015.
Original Russian Text © A.T. Baryshnikova, B.F. Minaev, G.V. Baryshnikov, Wen-Hua Sun, 2015, published in Zhurnal Neorganicheskoi Khimii, 2015, Vol. 60, No. 12, pp. 1703–1711.

PHYSICAL METHODS OF INVESTIGATION

Structure and Spectral and Luminescence Properties of the Trinuclear Zinc Complex with (*E*)-5-((2,6-Diethylphenylimino)methyl)-2-methylquinolin-8-ol: Experimental and DFT Study

A. T. Baryshnikova[a], B. F. Minaev[a, b], G. V. Baryshnikov[a], and Wen-Hua Sun[b]

[a] *National Bohdan Khmelnytsky University of Cherkassy, ul. Shevchenko 81, Cherkassy, 18031 Ukraine*
e-mail: glebchem@rambler.ru

[b] *Key Laboratory of Engineering Plastics, Institute of Chemistry, Chinese Academy of Sciences, and Beijing National Laboratory of Molecular Sciences, Beijing, China*
e-mail: whsun@iccas.ac.cn

Received February 26, 2015

Abstract—Quantum chemical optimization of the equilibrium structure of the trinuclear zinc complex with (*E*)-5-((2,6-diethylphenylimino)methyl)-2-methylquinolin-8-ol at the density functional theory level followed by Bader analysis of the electron density distribution function was performed on the basis of X-ray diffraction data for the molecular crystals of the complex. Interpretation of the topological parameters of electron density in the critical points of the Zn–O and Zn–N coordination bonds was carried out and the energies of these bonds were estimated using the Espinosa formula. Calculations in terms of the non-stationary density functional theory were used to simulate the absorption spectra of the complex and the structure-forming quinoline ligand. The $S_0 \rightarrow S_1$ transition subsequently responsible for generation of fluorescence is practically forbidden in the spectrum of the quinoline ligand and becomes allowed in the spectrum of the complex, which is observed experimentally as a fivefold enhancement of the quantum yield of fluorescence of the complex as compared with the ligand.

DOI: 10.1134/S0036023615120050

Polynuclear zinc complexes with N^O and N^N ligands have been subjects of intense research in recent years [1–4]. This is due, first of all, to their catalytic activity (including the biocatalytic properties of Zn-containing enzymes) and cytotoxicity [1–3]. Recently, it has been reported that polynuclear zinc complexes can serve as porous materials for gas storage [5]. However, most intriguing is the application of polynuclear zinc complexes as luminescent materials for the fabrication of organic light-emitting diodes (OLEDs) [6]. It is symptomatic that Zn(II) complexes are devoid of the crystal field stabilization effect (d^{10} configuration) and, hence, the coordination sphere of Zn^{2+} ions can assume different shapes depending on the conformational features of the ligands [7]. Owing to this fact, the coordination chemistry of zinc is highly diverse, which apparently accounts for the ever increasing implementation of these complexes in the OLED technology [6].

Apart from zinc complexes, aluminum, indium, and gallium complexes with 8-hydroxyquinoline and its derivatives are also popular fluorophores widely used in the manufacture of OLEDs [8]. However, in our opinion, zinc complexes are least studied among these materials as regards the relationship between the structural details and spectral and luminescence properties. This communication presents a detailed quantum chemical analysis of the structure and UV/Vis spectra of the recently synthesized zinc complex with (*E*)-5-((2,6-diethylphenylimino)methyl)-2-methylquinolin-8-ol (below referred to as HL) in relationship with the experimentally determined structure and spectral and luminescence properties [9]. The obtained results of quantum chemical calculations can be useful for targeted synthesis of new luminophores for OLEDs and for enhancing the properties of known Zn(II) complexes.

CALCULATION METHOD

A specific feature of the quantum chemical calculations presented in this study is full geometry optimization for the complex $[Zn_3L_6]$ (Fig. 1), which consists of 273 atoms and has no symmetry elements.

The geometries of $[Zn_3L_6]$ and the free ligand HL (Fig. 1) were optimized in terms of the density functional theory (DFT) using the exchange correlation functional B3LYP [10, 11] and the all-electron atomic orbital basis set DGDZVP [12, 13] for Zn atoms and the 6-31G(d) basis set [14] for C, N, O, and H atoms.

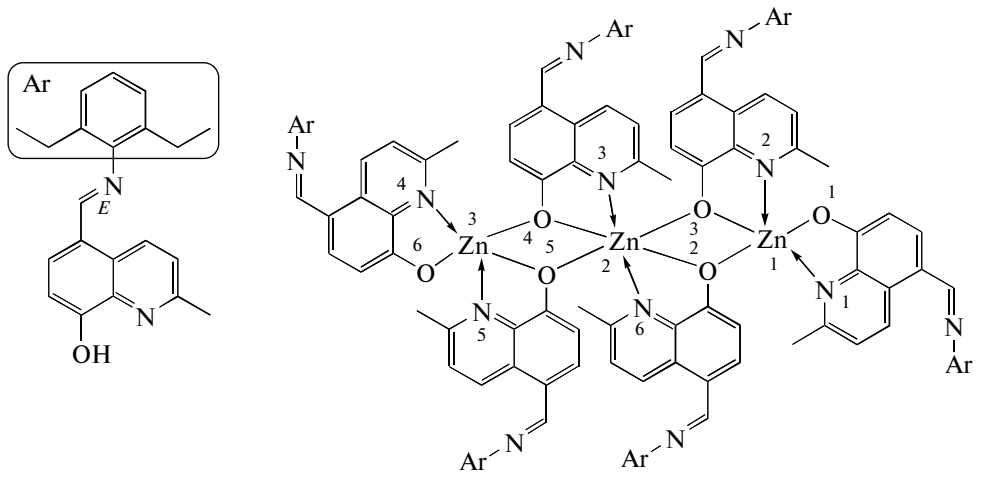

Fig. 1. Structure of the Zn(II) complex with (*E*)-5-((2,6-diethylphenylimino)methyl)quinolin-8-ol and atom numbering in the Zn(II) coordination spheres accepted in the paper.

Further analysis of the electron density distribution function $\rho(\mathbf{r})$ in the complex was performed within the framework of the Bader quantum theory "Atoms in Molecules" (QTAIM) [15]. The energies of coordinated and non-valence intramolecular bonds were estimated using the Espinosa formula [16, 17]:

$$E = \frac{1}{2} v(\mathbf{r}), \quad (1)$$

where $v(\mathbf{r})$ is the potential energy density in the specified bond critical point of the (3, −1) type (detailed information on the types of critical points of molecular structures and their physical meaning is given in [15, 18, 19]).

For the optimized geometry of the complex $[Zn_3L_6]$, thirty vertical singlet–singlet electronic transitions were calculated using the time-dependent density functional theory (TD-DFT) [20] with the same B3LYP functional and the DGDZVP/6-31G(d) basis sets. For the free ligand, we calculated forty vertical singlet–singlet electronic transitions in a similar approximation. The calculation was performed in a vacuum approximation and using the PCM solvation model [21] (model solvents were methanol, tetrahydrofuran (THF), and toluene, which were used for experimental recording of the absorption spectra of the complex and the ligand HL) [9].

The profiles of the simulated UV/Vis spectra of $[Zn_3L_6]$ and HL were constructed by means of the SWizard 4.6 program [22] using the Gaussian distribution function (line half-width is 3000 cm^{-1}). Quantum chemical DFT and TD-DFT calculations were carried out by means of the Gaussian09 program package [23]. The topological analysis of the electron density distribution function $\rho(\mathbf{r})$ was carried out by the AIMQB program implemented in the AIMAll computing package [24].

RESULTS AND DISCUSSION

Coordination details of the complex $[Zn_3L_6]$

According to X-ray diffraction data [9], the complex $[Zn_3L_6]$ has a trinuclear structure, two zinc cations being coordinated to three ligands by five bonds and the central zinc ion being coordinated to four ligands by six bonds. Each ligand is deprotonated upon complexation and, hence, they counterbalance the charge of the zinc ions. The coordination polyhedron of the pentacoordinated Zn1 and Zn3 ions is a distorted square pyramid with $O_1O_2O_3N_1$ and $O_5O_4O_6N_5$ bases (Fig. 2), whereas the hexacoordinated Zn2 ion has a quasi-octahedral environment with vertices at N6 and O3. Both types of coordination polyhedra are well known for zinc complexes [7, 25], although they are much less often encountered than tetrahedral complexes [26–28].

The complex $[Zn_3L_6]$ can actually be considered as a trimer of the complex ZnL_2, the simplest analog of which is the well-known luminophore ZnQ_2 (Q is the 8-hydroxyquinoline anion) [8, 29]. The possibility of oligomerization of ZnQ_2 has been repeatedly studied both experimentally [30–32] and by quantum chemical approximations [33]. It was shown that oligomeric complexes such as $(ZnQ_2)_2$, $(ZnQ_2)_3$, and $(ZnQ_2)_4$ are indeed formed both in solutions and in the condensed phase to give nanorods possessing luminophore properties [31–33]. In particular, it was found [31] that heating in vacuum to 180°C gives mainly $(ZnQ_2)_4$ with minor amounts of the other oligomers. In [33], it was shown that the conformation of the complex $(ZnQ_2)_4$ is sensitive to the substituents in the quinoline moiety.

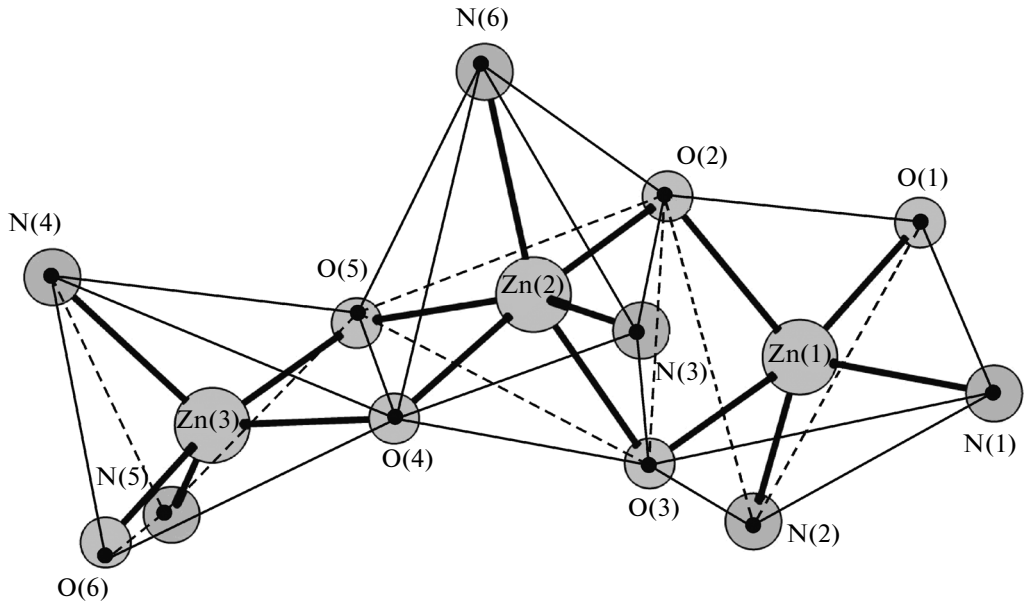

Fig. 2. Shape of the Zn(II) coordination polyhedra in the complex $[Zn_3L_6]$. The atom numbering is the same as in Fig. 1.

Similar conclusions are valid for the complex $[Zn_3L_6]$: its coordination structure (Fig. 2) substantially differs from that of the related complex $(ZnQ_2)_3$ (Fig. 2c in [33]) devoid of the –CNAr substituent in position 5 of 8-hydroxyquinoline. Conversely, the conformation of $[Zn_3L_6]$ is in good agreement with the structures of trinuclear zinc complexes with (*E*)-2-(2-arylethynyl)-8-hydroxyquinolines, which have bulky substituents in position 2 of the quinoline nucleus [34].

Trimerization of the complex ZnL_2, like the oligomerization of the related complexes ZnQ_2 [32] and $Zn(ppo)_2$ (ppo is the 2-(2-hydroxyphenyl)-5-phenyl-1,3-oxazole anion) [35], occurs via the formation of three-center oxygen bridges between the zinc atoms ($Zn_3O_4Zn_2$, $Zn_3O_5Zn_2$, $Zn_1O_2Zn_2$, and $Zn_1O_3Zn_2$), the Zn–O bonds in each bridge being inequivalent in the length and topological electron density distribution parameters (Table 1). The shorter Zn_3O_5, Zn_1O_3, Zn_2O_2, and Zn_2O_4 bonds (type 1) are about 2.056–2.063 Å long according to calculations and are identical in pairs (Table 1), which is in good agreement with X-ray diffraction data [9]. The Zn_1O_2, Zn_3O_4, Zn_2O_5, and Zn_2O_3 (type 2) bonds are longer (calcd.: 2.151–2.222 Å) and are also identical in pairs. The coordination spheres of Zn_3 and Zn_1 ions also have the shortest Zn_1O_1 and Zn_3O_6 distances (type 3) with calculated lengths of ~2.004 Å (Table 1), which correspond to the ligands not involved in the simultaneous coordination with two zinc ions (Figs. 1, 2).

The energy Zn–O bonds of types 1 and 3 estimated from formula (1) is about 30–40 kcal/mol depending on the interatomic distance. These bonds have high $\rho(\mathbf{r})$ values and positive Laplacians $\nabla^2\rho(\mathbf{r})$; the potential energy density $\nu(\mathbf{r})$ for them prevails over the kinetic energy density $g(\mathbf{r})$, while the resultant electronic energy density $h_e(\mathbf{r})$ is negative. The ratio of curvature elements $\left|\frac{\lambda_1}{\lambda_3}\right|$ for these bonds is considerably less than unity [15]. Thus, according to all indications, the Zn–O bonds of types 1 and 3 correspond to the intermediate type of interaction in terms of the Bader formalism [15, 18, 19]. These bonds are characterized by a high degree of covalency, as indicated by the high electron density delocalization index (DI = 0.3–0.4) for the interatomic space (Table 1).

Unlike type 1 and 3 bonds, in the Zn–O bonds of type 2, due to longer interatomic distance, the kinetic energy density $g(\mathbf{r})$ prevails over the potential energy density $\nu(\mathbf{r})$. Thus, $|g(\mathbf{r})| > |\nu(\mathbf{r})|$, which is typical of weak interactions between closed shells (this implies that the electron density is mainly concentrated in the near-nucleus space of separate atoms and is highly rarefied between them toward the bond). As a consequence, the covalency of type 2 bonds is substantially lower compared to type 1 and 3 bonds and the estimated bond energy for type 2 bonds is only 17–22 kcal/mol.

The coordination sphere of each Zn^{2+} ion in $[Zn_3L_6]$ is completed by two Zn–N bonds (altogether 6 bonds). Due to hybridization, all Zn–N bonds are almost identical for the pentacoordinated Zn1 and Zn3 ions (Zn_1N_2, Zn_3N_4, Zn_1N_1, and Zn_1N_5) and have roughly the same topological characteristics (Table 1), namely, they are intermediate type interactions, like most strong coordination bonds [7, 26, 27]. Two bonds, Zn_2N_6 and Zn_2N_3, which coordinate the Zn2 ion are also virtually equivalent; however, they

Table 1. Coordination bond lengths (d), energies (E), and topological characteristics of the electron density distribution in the bond critical points of type (3, −1) of $[Zn_3L_6]$

Bond	d, Å	d_{exp}, Å	$\rho(\mathbf{r})$, ea_0^{-3}*	$\nu(\mathbf{r})$, au	$g(\mathbf{r})$, au	$h_e(\mathbf{r})$**, au	$\nabla^2\rho(\mathbf{r})$, ea_0^{-5}	E, kcal/mol	$\lvert\lambda_1\rvert/\lvert\lambda_3\rvert$	ε	DI
Zn3O5	2.056	2.021	0.0667	−0.1088	0.1018	−0.0070	0.3789	−34.1	0.166	0.06	0.331
Zn1O3	2.062	2.019	0.0660	−0.1067	0.1001	−0.0066	0.3738	−33.5	0.166	0.06	0.326
Zn3O6	2.005	1.983	0.0759	−0.1319	0.1192	−0.0127	0.4258	−41.4	0.170	0.05	0.383
Zn1O1	2.004	1.956									
Zn2O4	2.063	2.026	0.0652	−0.1062	0.0999	−0.0063	0.3747	−33.3	0.164	0.05	0.307
Zn2O2	2.063	2.040									
Zn3O4	2.159	2.072	0.0486	−0.0691	0.0712	0.0021	0.2930	−21.7	0.150	0.07	0.253
Zn1O2	2.151	2.066	0.0493	−0.0708	0.0727	0.0019	0.2985	−22.2	0.151	0.07	0.256
Zn3N5	2.176	2.136	0.0578	−0.0805	0.0763	−0.0042	0.2886	−25.2	0.169	0.05	0.335
Zn1N1	2.176	2.172									
Zn3N4	2.169	2.143	0.0588	−0.0825	0.0777	−0.0048	0.2918	−25.9	0.170	0.04	0.332
Zn1N2	2.169	2.168									
Zn2N3	2.232	2.135	0.0507	−0.0651	0.0644	−0.0007	0.2551	−20.4	0.163	0.01	0.276
Zn2N6	2.224	2.140	0.0515	−0.0668	0.0658	−0.0010	0.2594	−21.0	0.164	0.01	0.279
Zn2O5	2.221	2.143	0.0421	−0.0547	0.0582	0.0035	0.2467	−17.2	0.150	0.06	0.197
Zn2O3	2.222	2.143									

* a_0 is the Bohr radius;
** $h_e(\mathbf{r}) = \nu(\mathbf{r}) + g(\mathbf{r})$.

have a calculated length of about 2.22 Å, which is somewhat longer than for other Zn–N bonds (calcd.: average 2.17 Å). Hence, the Zn_2N_6 and Zn_2N_3 bond energy is almost 5 kcal/mol lower; however, the intermediate type of interaction is retained (the ratio $|g(\mathbf{r})| < |\nu(\mathbf{r})|$ holds, whereas $\nabla^2\rho(\mathbf{r}) > 0$).

The performed detailed analysis of the energies of the Zn–O and Zn–N coordination bonds implies, first of all, high thermal stability of this complex. In addition, the obtained data on the energy differences between particular coordination bonds can be verified in a precision thermogravimetric experiment and subsequently used to analyze the destruction pathways of the complex.

Spectral and luminescence properties of HL and $[Zn_3L_6]$

As shown in a number of studies [36, 37], the electron transition to the first excited singlet state (S_1) of unsubstituted 8-hydroxyquinoline has a low intensity. Therefore, this compound has a rather low fluorescence [37]. Quenching of 8-hydroxyquinoline fluorescence is also promoted by the intramolecular proton transfer in the S_1 state (OH → N) [37], resulting in the electronically excited molecules in the non-fluorescent ketone form. In our case, the first excited S_1 state of the free ligand (*E*)-5-((2,6-diethylphenylimino)methyl)-2-methylquinolin-8-ol (HL) is also fluorescence-inactive. According to calculations, this is attributable to the fact that this state is due to charge transfer from the diethylphenylimine to quinoline moiety of HL, i.e., this corresponds to electron transition from the highest occupied molecular orbital (HOMO) to the lowest unoccupied orbital (LUMO) (Fig. 3). These moieties are perpendicular in space; therefore, the HOMO and LUMO wave functions do not have common overlap areas and the resultant transition dipole moment and the oscillator strength are virtually zero (Table 2).

It is characteristic that in $[Zn_3L_6]$, the wave functions of the spectrally active MO (HOMO–HOMO-5) are delocalized over both the diethylphenylimine and quinoline moieties of the ligands, while the frontier vacant MOs are localized only on the quinoline parts of these ligands. Thus, the low-lying excited states of $[Zn_3L_6]$ (Table 2) are due to charge transfer from the diethylphenylimine to quinoline moiety of the ligand, which is clearly seen in Fig. 4. For example, the main configuration for the S_1 state of the complex is HOMO-2 → LUMO (Table 2, Fig. 4). These two orbitals have a common electron density localization area, which is concentrated on the quinoline moiety. Therefore, the dipole moment of the $S_0 \rightarrow S_1$ transition

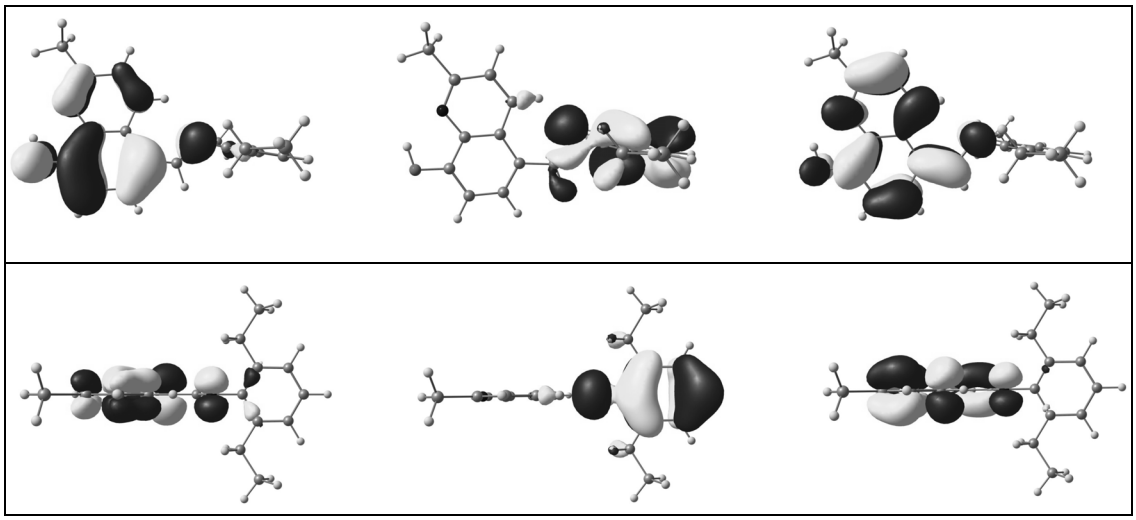

Fig. 3. B3LYP/6-31G(d)-calculated shape of frontier molecular orbitals of the HL molecule. The isocontour value is 0.03 a.u.

is non-zero and the corresponding oscillator strength is rather high (0.06–0.09). This conclusion is supported experimentally [9] as a substantial enhancement of the fluorescence quantum yield for the complex as compared with the initial ligand.

According to our calculated and experimental data, the complex formation with Zn(II) ions leads to a red shift of the first absorption band in the UV/Vis spectrum of $[Zn_3L_6]$ (Fig. 5) with respect to the spectrum of the ligand HL (Fig. 6). The same is observed

Table 2. Calculated spectral characteristics of the complex $[Zn_3L_6]$ and the ligand HL: vertical electronic transition wavelengths (λ, nm), oscillator strengths (*f*), and assignment of electronic transitions with contributions of the relevant configurations. The values in parentheses are experimental results [9]

	ES	λ, nm	*f*	Assignment
		THF		
HL	S_1	382	1×10^{-4}	HOMO → LUMO (96%)
	S_2	335 (334)	0.346	HOMO-1 → LUMO (95%)
$[Zn_3L_6]$	S_1	423	0.090	HOMO-2 → LUMO (55%)
				HOMO → LUMO (27%)
	S_8	403 (409)	0.299	HOMO-2 → LUMO+1 (48%)
				HOMO-2 → LUMO+3 (17%)
		Methanol		
HL	S_1	380	1×10^{-4}	HOMO → LUMO (96%)
	S_2	333 (334)	0.337	HOMO-1 → LUMO (95%)
$[Zn_3L_6]$	S_1	421	0.087	HOMO-2 → LUMO (55%)
				HOMO → LUMO (26%)
	S_8	401 (392)	0.339	HOMO-2 → LUMO+1 (50%)
				HOMO-2 → LUMO+3 (14%)
		Toluene		
HL	S_1	387	1×10^{-4}	HOMO → LUMO (96%)
	S_2	337 (335)	0.350	HOMO-1 → LUMO (95%)
$[Zn_3L_6]$	S_1	428	0.063	HOMO → LUMO (49%)
				HOMO-2 → LUMO (34%)
	S_8	406 (415)	0.216	HOMO-2 → LUMO+1 (41%)
				HOMO-2 → LUMO+3 (21%)

* Data are given for the first singlet (S_1) excited state (ES) and for the most intense transitions in the spectra of HL and $[Zn_3L_6]$ to the S_2 and S_8 states, respectively, which form the first (long-wavelength) absorption band in the observed spectra.

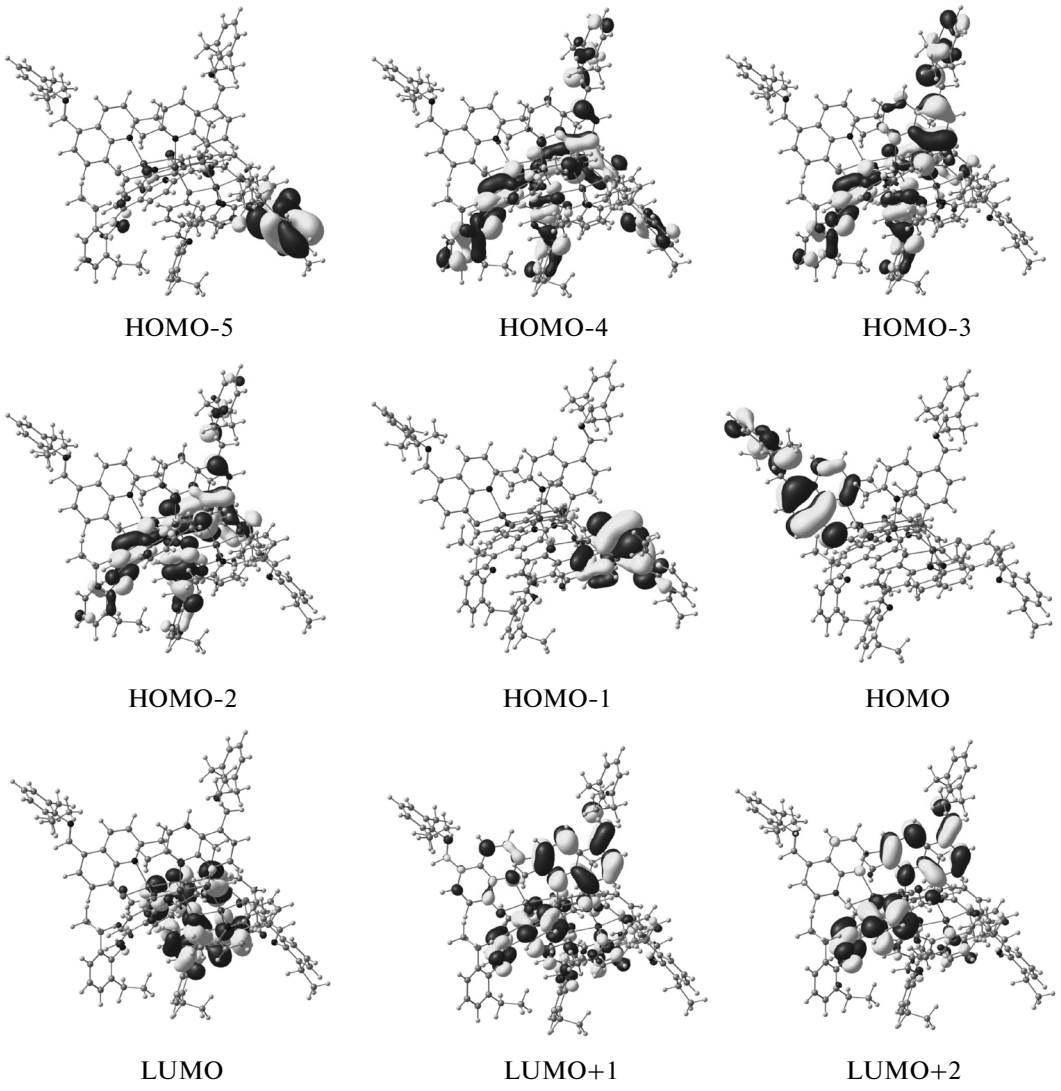

Fig. 4. Shapes of some spectrally active molecular orbitals of $[Zn_3L_6]$ calculated by B3LYP/DGDZVP (Zn)/6-31G(d) (N, O, C, H). The isocontour value is 0.03 a.u.

for some other synthesized Zn(II) complexes with 8-hydroxyquinoline derivatives [38, 39] and with Schiff bases [40, 41]. Calculations show that the red shift is caused, first of all, by the strong destabilization of the occupied MOs upon complex formation: their energy increases by more than 0.5 eV, while the energy of the corresponding vacant MOs in the complex decreases by ~0.1 eV. All this is in line with the observed red shift of the first absorption band of the complex by 60–70 nm depending on the solvent polarity.

Note that, according to calculation results, the energies of the excited states of the free ligand do not depend on the solvent polarity, which is considered in terms of the polarizable continuum model (PCM). Experimental investigations [9] also attest to the absence of solvatochromic effect for the first absorption band of HL. For the complex $[Zn_3L_6]$, the effect of solvent on the position of the first absorption maximum and the energy of the first S_1 state is more noticeable and is manifested as a red shift following the decrease in the solvent polarity. For example, for the series of solvents: methanol (dielectric permittivity $\varepsilon = 32.6$), THF ($\varepsilon = 7.4$), and toluene ($\varepsilon = 2.4$), the first absorption maxima of the complex are experimentally identified at 392, 403, and 406 nm, respectively. This effect can also be followed in the calculated data, although the solvatochromic shift is smaller in this case (Table 2).

Thus, the quantum chemical analysis at the TD-DFT level of the observed spectral and luminescence properties of the zinc complex with (*E*)-5-((2,6-diethylphenylimino)methyl)-2-methylquinolin-8-ol demonstrated good qualitative and quantitative agreement with experimental data and accounted for the experimentally observed increase in the fluorescence quantum yield of the complex with respect to the free

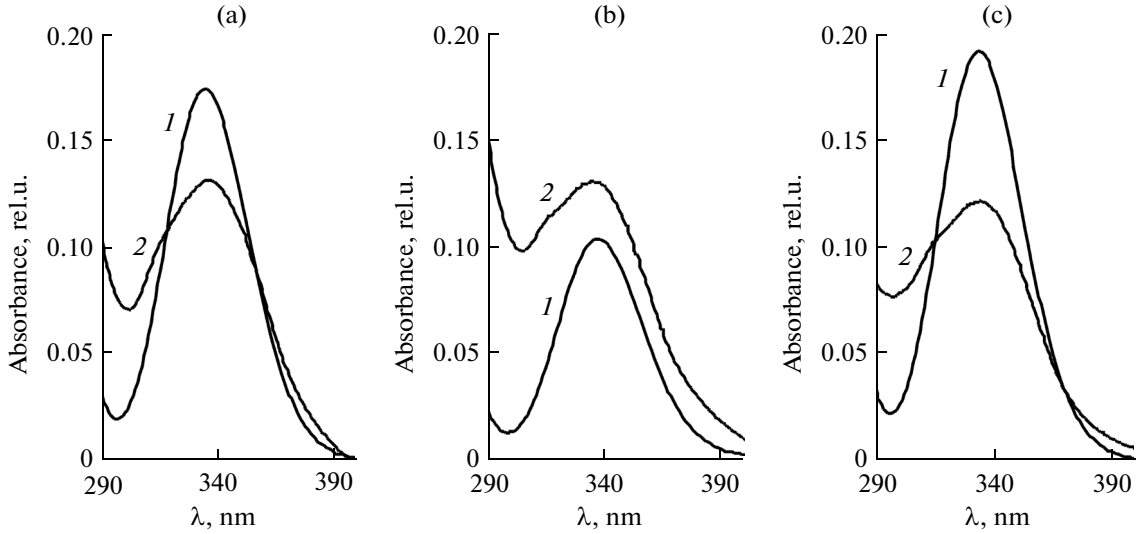

Fig. 5. UV/Vis spectra of the HL molecule: (*1*) simulated curves, (*2*) experimental curves [9]; (a) THF as the solvent, (b) toluene as the solvent, (c) methanol as the solvent.

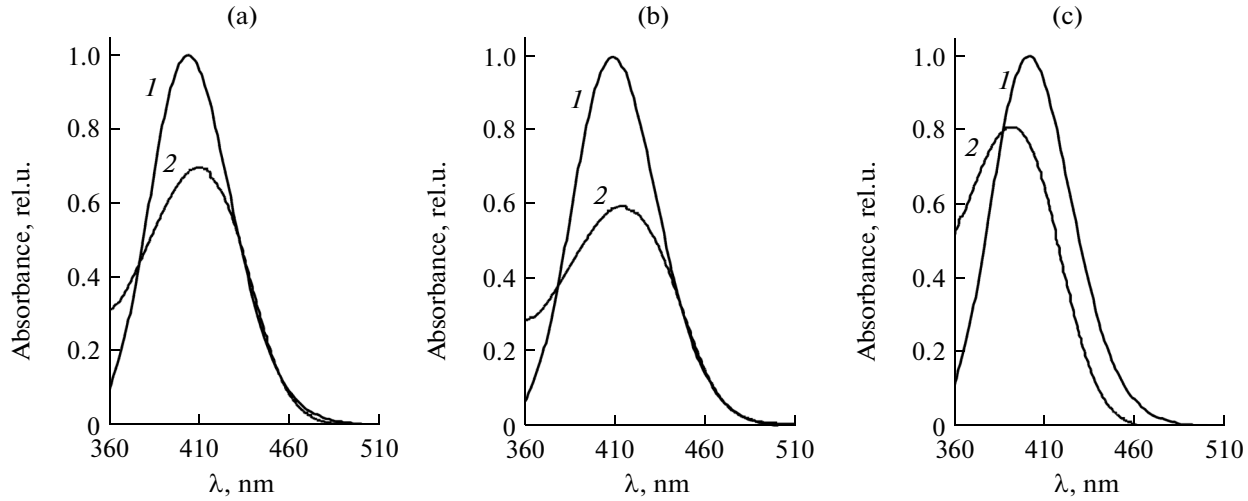

Fig. 6. UV/Vis spectra of the complex $[Zn_3L_6]$. For designations, see Fig. 5.

ligand. In view of the determined spectral and luminescence characteristics in combination with high thermal stability, the complex $[Zn_3L_6]$ can be regarded as a promising fluorophore for organic light-emitting diodes. The use of this complex as a host material for the fabrication of multiemission OLEDs also seems quite promising.

CONCLUSION

The trinuclear zinc complex with (*E*)-5-((2,6-diethylphenylimino)methyl)-2-methylquinolin-8-ol is of fundamental and practical interest due to its unusual stereochemistry and high fluorescence efficiency. In particular, it was shown that the presence of bulky substituents in position 5 of the quinoline nucleus causes a change in the mode of ligand coordination to the central zinc ions with respect to that in related complexes without substituents. Estimation of the energies of the Zn–O and Zn–N coordination bonds demonstrates high stability of the complex in question and implies the rigid molecular skeleton of the whole compound, which decreases the fluorescence quenching via vibrational relaxation of the electronically excited states.

The TD-DFT simulation of the absorption spectra of the complex and the free ligand revealed the nature of the charge transfer for the first singlet excited state of these molecules and provided explanation for enhancement of the fluorescence efficiency of the complex. Analysis of the shapes of molecular orbitals

showed that the ligand transition to the S_1 state is symmetry forbidden; this is reduced to the superimposition of the more intense transition to the S_2 state on the first absorption band. This is also experimentally observed as a low fluorescence quantum yield of the ligand ($\Phi = 0.14$ in methanol). The vertical transition to the S_1 state for the zinc complex is much more intense due to delocalization of the spectrally active HOMO-2 and LUMO, which embrace simultaneously several ligands, including the diethylphenylimine and quinoline moieties; this accounts for the high observed fluorescence quantum yield of the complex ($\Phi = 0.68$ in methanol).

ACKNOWLEDGMENTS

This work was supported by the Ministry of Science and Educatuin of Ukraune (basic research project no. 0115U000637). B.F. Minaev gratefully acknowledges the support of the Foundation of the President of the Academy of Sciences of China in the framework of its international initiative.

REFERENCES

1. T. Arai, N. Sugiyama, H. Masu, et al., Chem. Commun. **50**, 8287 (2014).
2. D. Dey, G. Kaur, A. Ranjani, et al., Eur. J. Inorg. Chem. **2014**, 3350 (2014).
3. X. Liu, P. Du, and R. Cao, Nat. Commun. **4**, 2375 (2013).
4. D. J. D. Wilson, C. M. Beavers, and A. F. Richards, Eur. J. Inorg. Chem. **2012**, 1130 (2012).
5. B. Wang, A. P. Côté, and H. Furukawa, Nature **453**, 207 (2008).
6. F. Dumur, Synth. Met. **195**, 241 (2014).
7. G. V. Baryshnikov, B. F. Minaev, A. A. Korop, et al., Russ. J. Inorg. Chem. **58**, 928 (2013).
8. H. Xu, R. Chen, Q. Sun, et al., Chem. Soc. Rev. **43** (10), 3259 (2014).
9. Q. Yan, L. Li, W. Li, et al., Spectrochim. Acta A **128**, 790 (2014).
10. A. D. Becke, J. Chem. Phys. **98**, 5648 (1993).
11. C. Lee, W. Yang, and R. G. Parr, Phys. Rev. B **37**, 785 (1988).
12. N. Godbout, D. R. Salahub, J. Andzelm, et al., Can. J. Chem. **70**, 560 (1992).
13. C. Sosa, J. Andzelm, B. C. Elkin, et al., J. Phys. Chem. **96**, 6630 (1992).
14. M. M. Francl, W. J. Petro, W. J. Hehre, et al., J. Chem. Phys. **77**, 3654 (1982).
15. R. F. W. Bader, *Atoms in Molecules. A Quantum Theory* (Clarendon Press, Oxford, 1990).
16. E. Espinosa, E. Molins, and C. Lecomte, Chem. Phys. Lett. **285**, 170 (1998).
17. E. Espinosa, I. Alkorta, and I. Rozas, Chem. Phys. Lett. **336**, 457 (2001).
18. I. S. Bushmarinov, K. A. Lyssenko, and M. Yu. Antipin, Russ. Chem. Rev. **78**, 283 (2009).
19. G. V. Baryshnikov, B. F. Minaev, V. A. Minaeva, et al., Russ. J. Gen. Chem. **81**, 576 (2011).
20. E. Runge and E. K. U. Gross, Phys. Rev. Lett. **52**, 997 (1984).
21. S. Miertus, E. Scrocco, and J. Tomasi, Chem. Phys. **55**, 117 (1981).
22. S. I. Gorelsky, SWizard program, rev. 4.6, Univ. of Ottava, Canada, 2010.
23. M. J. Frisch, G. W. Trucks, H. B. Schlegel, et al., GAUSSIAN09, rev. A.02, Gaussian, Inc., Wallingford, CT, 2009.
24. T. A. Keith, AIMAll (ver. 10.07.25), TK Gristmill Software, Overland Park KS, USA. www.aim.tkgristmill.com, 2010.
25. V. A. Minaeva, B. F. Minaev, G. V. Baryshnikov, et al., Russ. J. Gen. Chem. **81**, 2332 (2011).
26. B. F. Minaev, G. V. Baryshnikov, A. A. Korop, et al., Opt. Spectrosc. **113**, 298 (2012).
27. B. F. Minaev, G. V. Baryshnikov, and A. A. Korop, Opt. Spectrosc. **114**, 30 (2013).
28. R. R. Valiev, E. N. Telminov, T. A. Solodova, et al., Spectrochim. Acta A **128**, 137 (2014).
29. Y. Hamada, T. Sano, M. Fujita, et al., Jpn. J. Appl. Phys. **32** (4A), L514 (1993).
30. V. K. Shukla and J. Maitra, J. Mater. **2013**,ID 690237 (2013).
31. X. Bing-she, H. Yu-ying, W. Hua, et al., Solid State Commun. **136**, 318 (2005).
32. L. S. Sapochak, F. E. Benincasa, R. S. Schofield, et al., J. Am. Chem. Soc. **124**, 6119 (2002).
33. L. S. Sapochak, A. Falkowitz, K. F. Ferris, et al., J. Phys. Chem. B **108**, 8558 (2002).
34. G. Yuan, Y. Huo, X. Nie, et al., Dalton. Trans. **42**, 2921 (2013).
35. T. S. Kim, T. Okubo, and T. Mitani, Chem. Mater. **15**, 4949 (2003).
36. S.-C. Lan and Y.-H. Liu, Spectrochim. Acta A **139**, 49 (2015).
37. M. Amati, S. Belviso, P. L. Cristinziano, et al., J. Phys. Chem. A **111**, 13403 (2007).
38. A. Kumar, A. K. Palai, R. Srivastava, et al., J. Organomet. Chem. **756**, 38 (2014).
39. S. Li, Y. Li, and J.-A. Zhang, Inorg. Chem. Commun. **20**, 334 (2012).
40. L. Li, X. Zhang, W. Zhang, et al., Spectrochim. Acta A **118**, 1047 (2014).
41. O. V. Kotova, S. V. Eliseeva, A. S. Averjushkin, et al., Russ. Chem. Bull. **57**, 1880.

Translated by Z. Svitanko